ISSN 1070-3632, Russian Journal of General Chemistry, 2015, Vol. 85, No. 6, pp. 1370–1375. © Pleiades Publishing, Ltd., 2015.
Original Russian Text © V.I. Popkov, O.V. Almjasheva, M.P. Schmidt, V.V. Gusarov, 2015, published in Zhurnal Obshchei Khimii, 2015, Vol. 85, No. 6, pp. 901–907.

Formation Mechanism of Nanocrystalline Yttrium Orthoferrite under Heat Treatment of the Coprecipitated Hydroxides

V. I. Popkov, O. V. Almjasheva, M. P. Schmidt, and V. V. Gusarov

St. Petersburg State Technological Institute (Technical University), Moskovskii pr. 26, St. Petersburg, 190013 Russia
e-mail: vadim.i.popkov@gmail.com

Received March 16, 2015

Abstract—Formation of nanocrystalline yttrium orthoferrite of ~30 nm average crystallite size from coprecipitated iron(III) and yttrium hydroxides was studied by thermo-X-ray diffractometry and simultaneous thermal analysis over 25–900°C temperature range. A mechanism of physicochemical transformations leading to the formation of $YFeO_3$ nanoparticles was suggested.

Keywords: coprecipitation, yttrium orthoferrite, nanoparticles, heat treatment, phase formation

DOI: 10.1134/S107036321506002X

Yttrium orthoferrite ($YFeO_3$) is a perovskite-like compound possessing a broad range of properties making it attractive for advanced technical applications [1–4]. Nowadays many studies focus on the features of synthesis and properties of nanocrystalline $YFeO_3$ [5–10] with the view of developing new nanomaterials.

Preparation of nanoscale yttrium orthoferrite by the classical solid-phase reaction route is complicated by high temperatures and long time of synthesis required for these processes [11] where the formation of the target products, in particular, of perovskite orthoferrites [12, 13], may be accompanied by the appearance of impurity phases with crystallites growing to micron sizes. Such difficulties can be avoided by using "soft" synthesis methods [14], or other methods involving fast chemical reactions [15], including those based on combustion of the reactants [16, 17].

Although a considerable number of studies treats the methods of synthesis of nanocrystalline orthoferrites, there are only fragmentary data concerning the mechanisms of their formation from coprecipitated hydroxides [6, 17–20]. Still, the latter method is promising for the preparation of nanocrystals due to simple apparatus and positive experience of its application for high-speed synthesis of many oxide compounds, yielding nanocrystalline reaction products [15]. The synthesis of nanocrystalline yttrium orthoferrite by decomposition of coprecipitated hydroxides was considered in [6, 10], but the mechanism of its formation, whose knowledge would enable directed synthesis of nanocrystalline $YFeO_3$, still remains to be investigated.

The difficulty in investigating the mechanism of $YFeO_3$ formation from coprecipitated hydroxides consists in the multiplicity of chemical compounds and their polymorphs occurring in the Fe_2O_3–Y_2O_3–H_2O system [21–23]. This is responsible for high variance of the processes involved in dehydration and, consequently, for a strong effect exerted by the dehydration conditions on the chemical composition, structure, morphology, and dispersity of the final products. Moreover, high reactivity of the freshly precipitated yttrium hydroxide, which reacts with the atmospheric CO_2 to form hydroxycarbonates [9, 21], leads to chemical inhomogeneity of the coprecipitated substances and to the formation of impurity phases. In [24, 25], it was shown that the carbonation of coprecipitated hydroxides in air results in amorphization of the analyzed composition, but the influence of this process on phase formation was not discussed.

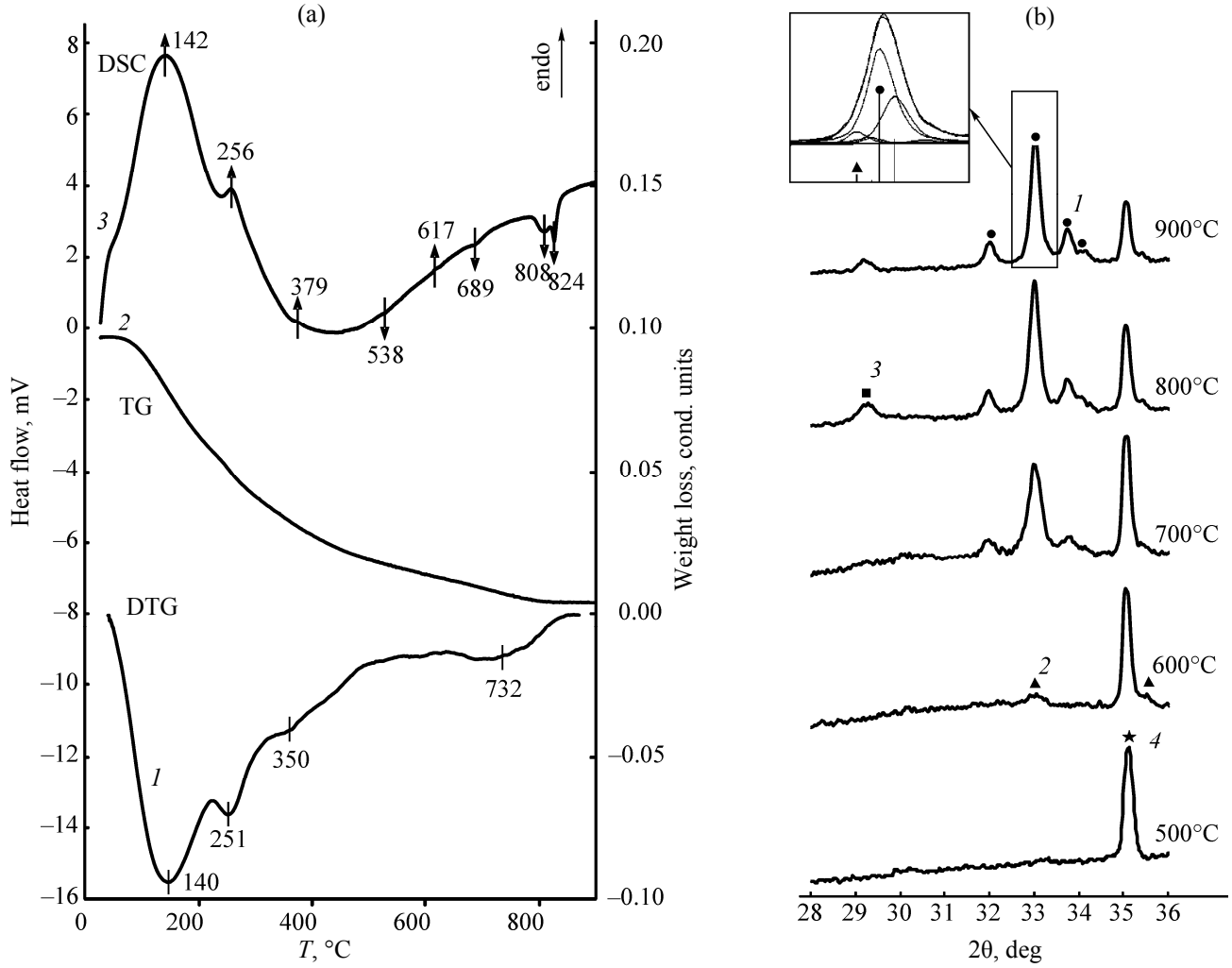

Fig. 1. Data of the transformations analysis of the coprecipitation products under heating: (a) simultaneous thermal analysis and (b) thermo-X-ray diffraction. Phases: (*1*) $YFeO_3$, (*2*) α-Fe_2O_3, (*3*) α-Y_2O_3, and (*4*) α-Al_2O_3 (internal standard).

Thus, both the mechanism of the formation of nanocrystalline yttrium orthoferrite from the coprecipitated hydroxides and the role of partial carbonation in this process remain unclear. Specifically these issues are mainly addressed in this study.

The reaction formulation was obtained by coprecipitation of iron(III) and yttrium hydroxides from their nitrate solutions with an ammonia solution, and this was followed by washing and drying in air. According to the X-ray microanalysis data, the elemental composition of the reaction formulation yielded by coprecipitation was 50.4±0.5 and 49.6±0.5 at % of iron and yttrium, respectively, which corresponds, within the accuracy of the analysis method, to the stoichiometric (50 : 50 at %) ratio of the elements, preset in the synthesis.

Figure 1 shows the results of simultaneous thermal analysis and thermo-X-ray diffractometry of the coprecipitated composition. These data suggest that, under the actual conditions, the orthoferrite formation involves a sequence of physicochemical transformations whose corresponding temperature range can be conditionally divided into two ranges. The first range, from room temperature to 500–600°C, is characterized by the largest weight loss in the TG curve and intense endothermic peaks in the DSC curve, while in the diffraction patterns X-ray reflections are totally absent up to 600°C. The second range, from 500–600°C to 900°C, exhibits low- and medium-intensity exothermic peaks associated with crystallization of the amorphous substance and the formation of new chemical compounds, as confirmed by X-ray diffraction data.

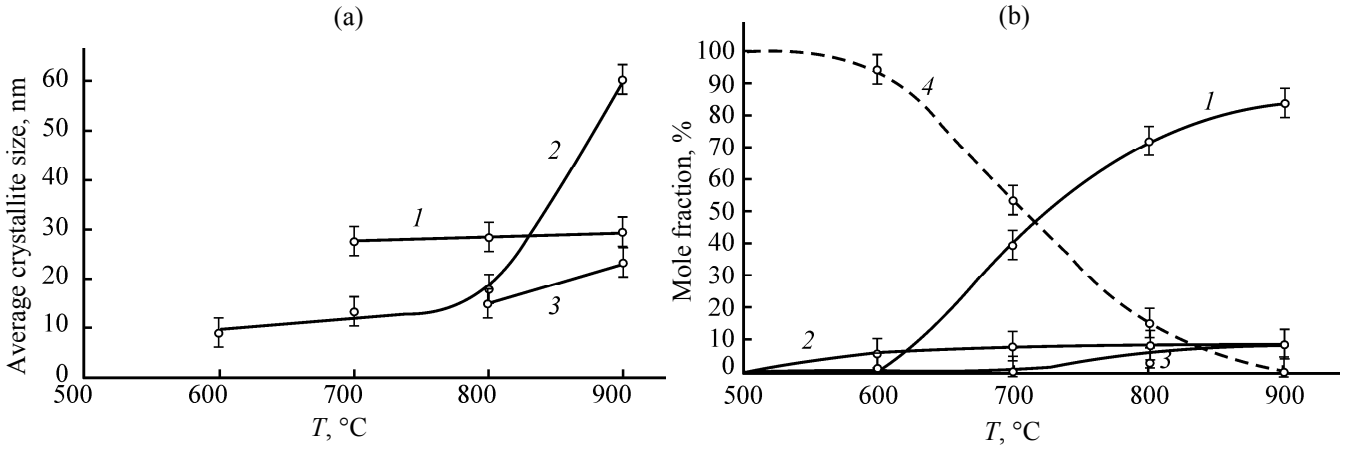

Fig. 2. Temperature dependence of (a) crystallite size and (b) quantitative ratio of the coexisting phases: (*1*) $YFeO_3$, (*2*) α-Fe_2O_3, (*3*) α-Y_2O_3, and (*4*) amorphous phase.

The weight loss in this range is insignificant compared to the first range.

It seems reasonable to consider the changes occurring in nanoscale systems taking into account the dispersity of the components and their content in the system. Accordingly, Fig. 2 presents the quantitative X-ray phase analysis data and the calculated crystallite sizes for the coexisting phases, derived from the X-ray diffraction data.

Comparing the simultaneous thermal analysis data, thermo-X-ray diffraction analysis results, and the available published data allowed us the following characterization of processes occurring during heat treatment of the coprecipitated hydroxides. The endothermic peaks with maxima at 142 and 256°C, corresponding to the DTG peaks in the same temperature ranges, evidence significant weight losses of 10.9±0.7 and 11.6±0.8%, respectively. The width and intensity of the observed peaks suggest that they describe the totality of the processes associated with both the vaporization of free and adsorbed water from the substance [22, 26, 27] and the decomposition of iron and yttrium hydroxides having low stability at elevated temperatures [26, 28]. The latter process is not manifested in the X-ray diffraction data, because the sample analyzed is X-ray amorphous to 500°C inclusive.

Another factor responsible for the weight losses in the sample is decomposition of yttrium hydroxycarbonate $Y_2(OH)_4CO_3$ and oxycarbonate $Y_2O_2CO_3$, respectively [9, 25], which appeared in the system because of high reactivity of the freshly precipitated yttrium hydroxide toward atmospheric carbon dioxide. These carbonation products do not show up in the X-ray diffraction pattern probably since they are highly amorphous. However, their decomposition causes low-intensity endothermic peaks with DTG maxima at 379 and 617°C and weight losses of 3.1±0.6 and 2.4±0.6% in the TG curves, observed for hydroxycarbonate and oxycarbonate, respectively. Based on the quantitative X-ray phase analysis data, the weight losses in the sample due to these processes were estimated at 2.0±0.5 and 2.5±0.5%, respectively, which findings coincide, within the limits of the measurement accuracy, with the thermal analysis data. This confirms the suggested sequence of the chemical reactions describing the transformations of the carbonation products of the precipitated yttrium hydroxide. It should be noted that, according to the TG analysis data, the yttrium oxycarbonate decomposition occurs over a very extended temperature range of 600–800°C, which complicates its recording in the DSC curve.

The DSC curve exhibits a weak exothermic peak at 538°C corresponding to the α-Fe_2O_3 crystallization [29], as confirmed by weak X-ray diffraction peaks at 600°C, observed at the 2θ angles corresponding to the most intense reflections from α-Fe_2O_3. With increasing temperature the detection of iron(III) oxide in the system from the X-ray diffraction pattern gets complicated by superposition of the reflections from other phases. However, a low-intensity peak at $2\theta \approx 35.5°$ corresponding to the (110) reflection from iron oxide with a hematite structure is indicative of the existence of α-Fe_2O_3 up to 900°C. It should be noted that, over the 600–900°C range, the amount of iron(III) oxide remains virtually unchanged, which may

indicate that the α-Fe_2O_3 formation is complete already at 600°C. In this process, the average size of the iron(III) oxide crystallites significantly increases as the temperature approaches the melting point of the two-dimensional non-autonomous phase, 997±180°C for iron(III) oxide [30]. The corresponding intensification of the recrystallization of the substance leads to a significant increase in the average size of the iron(III) oxide crystallites, from 15±3 to 60±7 nm.

The crystallization of α-Y_2O_3 proceeds at significantly higher temperatures. The most active stage of this process is accompanied by an exothermic peak in the DSC curve at 808°C. The yttrium oxide crystallization is also evidenced by the appearance of the corresponding reflection in the diffraction pattern at 800°C, broadly consistent with the data from [25]. Further increase in the heat-treatment temperature to 900°C does not noticeably affect the intensity of this reflection from α-Y_2O_3. It should be noted that the mole fraction of yttrium oxide in the system remains nearly unchanged over the 800–900°C temperature range, being numerically equal to that of α-Fe_2O_3 within the limits of the error in determining the quantitative composition of the sample. It presumably, the formation of simple oxides α-Fe_2O_3 and α-Y_2O_3 is due to inhomogeneity of the coprecipitated hydroxides, associated with their partial carbonation. In this case, the equality of the mole fractions of iron(III) and yttrium oxides in the system is explained by identity of the amounts of the iron- and yttrium-containing components that does not participate in the formation of yttrium orthoferrite, which originates from a homogeneous product of coprecipitation of the hydroxides, due to carbonation of the freshly precipitated yttrium hydroxide in air. A growing average size of the α-Y_2O_3 crystallites with temperature increasing from 800 to 900°C is apparently due to the recrystallization of yttrium oxide.

As known, precursors in the solid-phase synthesis of $YFeO_3$ are iron(III) and yttrium oxides. However, we observed only trace amounts of crystalline α-Fe_2O_3 and α-Y_2O_3 against significant amounts of the yttrium orthoferrite formed. Such behavior of the system suggests the existence of an alternative mechanism of the $YFeO_3$ formation without crystallization of the individual simple oxides. The formation of yttrium orthoferrite in this case can be regarded as a result of two parallel processes of physicochemical transformations. In one process, $YFeO_3$ is formed from a homogenous mixture of the coprecipitation products which undergo simultaneous dehydration without significant crystallization of intermediates. In the other process, the formation of yttrium orthoferrite becomes possible only after decomposition of the products of partial carbonation of the coprecipitated hydroxides into simple oxides.

This presumption is adequately supported by the simultaneous thermal analysis data. For example, in the DSC curve there are two exothermic effects with extrema at 689 and 824°C which can be associated with the $YFeO_3$ formation. At the lower of these temperatures, $YFeO_3$ is formed from the simultaneous dehydration products of the hydroxides; this process is manifested, along with the thermal effect in the DSC curve, in the appearance of reflections from $YFeO_3$ in the diffraction pattern at 700°C, being also in good agreement with published data [5]. At the higher of the temperatures, yttrium orthoferrite is evidently formed from the decomposition products of the carbonated part of the precursor, as indicated by the $YFeO_3$ formation onset temperature which falls within the temperature range of crystallization of yttrium oxide, with an exothermic peak at 808°C corresponding to its maximum rate. The fact that the processes of the $YFeO_3$ formation from the homogeneous part of the precursor and from the carbonation products of the coprecipitated hydroxides occur in parallel is indirectly confirmed by invariance, within the limits of the measurement accuracy, of the molar fractions of the simple oxides (α-Fe_2O_3 and α-Y_2O_3), while the molar fraction of $YFeO_3$ in the system is gradually increasing over the 600–900°C temperature range.

A relatively low temperature of the yttrium orthoferrite formation (~700°C) can be explained by high homogeneity of the initial mixture. This facilitates the transport of the reactants, so the $YFeO_3$ formation is limited only by structural transformations in the substance, with the average crystallite size of ~30 nm provided for $YFeO_3$.

On the other hand, the $YFeO_3$ formation from the simple oxides (α-Fe_2O_3 and α-Y_2O_3), which are the end products of the decomposition of the carbonated part of the precursor, is complicated because of the need in both the transformation of the structure of the system components and the mass transfer of the substances, with the latter factor being of decisive importance. Under these circumstances, the active mass transfer of the substance is possible at comparatively high temperatures which typically correlate with the melting point of the two-dimensional non-autonomous phase of

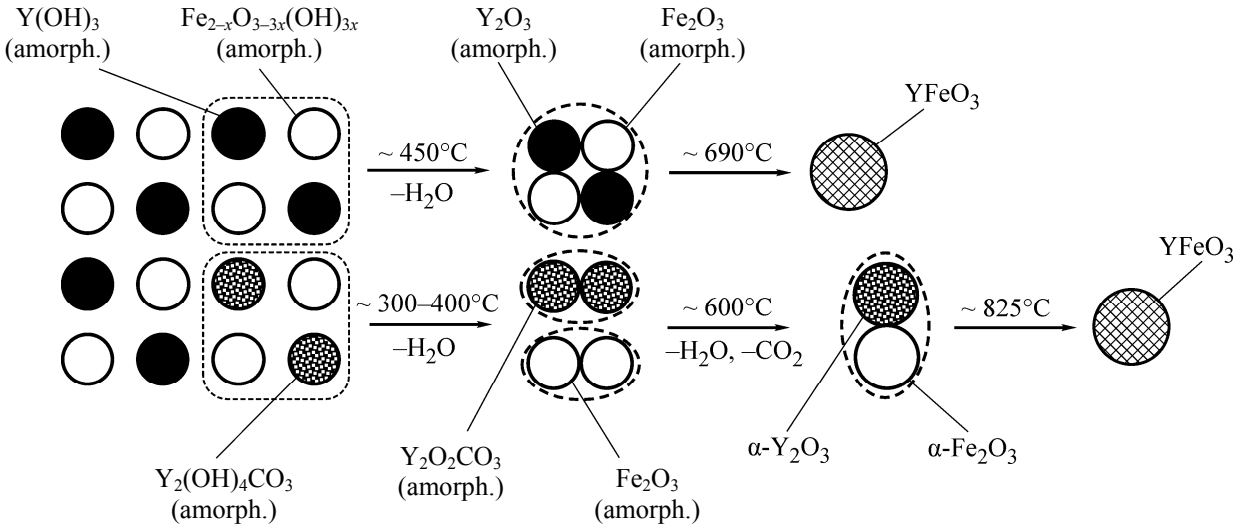

Fig. 3. Scheme of the chemical transformations occurring during heat treatment of the coprecipitation products.

the lower-melting reactant (α-Fe_2O_3). However, in this case the onset temperature of the yttrium orthoferrite formation is also affected by the formation of α-Y_2O_3 from $Y_2O_2CO_3$.

Thus, based on out research findings, the sequence of the physicochemical transformations leading to the yttrium orthoferrite formation by heat treatment of the coprecipitated hydroxides can be represented schematically as shown in Fig. 3.

In this study, heat treatment of the precursor, the coprecipitation product of iron(III) and yttrium hydroxides, resulted in the formation of the orthorhombic modification of yttrium orthoferrite with the average crystallite size of ~30 nm. It was shown that the $YFeO_3$ formation can follow two mechanisms: simultaneous dehydration of the coprecipitated hydroxides to give yttrium orthoferrite at temperatures near 690°C and separate decomposition of the carbonation products of the hydroxides to give yttrium orthoferrite at temperatures near 825°C. These processes involve various sequences of physicochemical transformations and are associated with chemical inhomogeneity of the precursor, arising in the coprecipitation stage. A total scheme of the physicochemical transformations leading to the formation of yttrium orthoferrite nanocrystals was suggested.

EXPERIMENTAL

The technique of preparation of mixed iron(III) and yttrium hydroxides by coprecipitation has been previously described in [9]. Iron(III) nitrate ("pure" grade) and yttrium nitrate ("pure" grade), taken in a 1 : 1 stoichiometric ratio, were dissolved in distilled water with vigorous stirring to obtain the solution of concentration 1 M in each of the components. Next, this solution was added dropwise to a vigorously stirred 1 M NaOH solution. Its acidity (pH) was 12, when the addition of the solution of the nitrates was complete. The resulting dark brown precipitate was filtered off and rinsed several times with distilled water until no sodium ions and nitrate ions could be detected. Next, the precipitate was dried at 70°C for several hours, after which it was thoroughly ground and analyzed.

The elemental composition was determined by X-ray microanalysis using a FEI Quanta 200 scanning electron microscope coupled with an EDAX energy dispersive analyzer. Simultaneous thermal analysis was performed in the differential scanning calorimetry-thermal gravimetry (DSC–TG) mode over the 25–900°C range using a Netzsch STA 449 F3 instrument.

Thermo-X-ray diffraction analysis was carried out in the 25–900°C temperature range using a Shimadzu XRD-7000 X-ray diffractometer (CuK_α-radiation, λ = 0.154051 nm) equipped with an Anton Paar HTK 1200N high-temperature chamber (time of treatment before measurement 30 min, measurement time ~12.5 min; measurement mode: Bragg's angle 25°–40°, scanning step 0.02°, measurement time at a point 1 s).

Qualitative X-ray phase analysis was performed using ICDD PDF2 powder diffraction data base [31].

Quantitative X-ray phase analysis was carried out by the Rietveld method [32]. The average crystallite size for the phases observed was calculated from the broadening of the X-ray diffraction lines using MAUD software package [33].

ACKNOWLEDGMENTS

This study was financially supported by the Russian Foundation for Basic Research (project no. 13-03-00888).

REFERENCES

1. Shen, H., Xu, J., Wu, A., Zhao, J., and Shi, M., *Mater. Sci. Eng., B*, 2009, vol. 157, nos. 1–3, p. 77. DOI: 10.1016/j.mseb. 2008.12.020.
2. Cheng, Z.X., Shen, H., Xu, J., Liu, P., and Zhang, S.J., *J. Appl. Phys*., 2012, vol. 111, no. 3, p. 034103-1. DOI: 10.1063/1.3681294.
3. Shang, M., Zhang, C., Zhang, T., Yuan, L., Ge, L., Yuan, H., and Feng, S., *Appl. Phys. Lett*., 2013, vol. 102, no. 6, p. 062903-1. DOI: 10.1063/1.4791697.
4. Zhang, R.-L., Chen, C.L., Jin, K.-X., Niu, L.-W., Xing, H., and Luo, B.-C., *J. Electroceram*., 2013, vol. 32, nos. 2–3, p. 187. DOI: 10.1007/s10832-013-9869-x.
5. Mathur, S., Veith, M., Rapalaviciute, R., Shen H., Goya, G.F., Filho, W.L.M., and Berquo, T.S., *Chem. Mater*., 2004, vol. 16, no. 10, p. 1906. DOI: 10.1021/cm0311729.
6. Tien, N.A., Almjasheva, O.V., Mittova, I.Ya., Stognei, O.V., and Soldatenko, S.A., *Inorg. Mater*., 2009, vol. 45, no. 11, p. 1304. DOI: 10.1134/S0020168509110211.
7. Tang, P., Chen, H., Cao, F., and Pan, G., *Catal. Sci. Technol*., 2011, vol. 1, no. 7, p. 1145. DOI: 10.1039/c1cy00199j.
8. Zhang, W., Fang, C., Yin, W., and Zeng, Y., *Mater. Chem. Phys*., 2013, vol. 137, no. 3, p. 877. DOI: 10.1016/j.matchemphys. 2012.10.029.
9. Popkov, V.I. and Almjasheva, O.V., *Nanosystems: Physics, Chemistry, Mathematics*, 2014, vol. 5, no. 5, p. 703.
10. Tien, N.A., Mittova, I.Ya., and Al'myasheva, O.V., *Russ. J. Appl. Chem*., 2009, vol. 82, no. 11, p. 1915. DOI: 10.1134/S1070427209110020.
11. Tret'yakov, Yu.D., *Tverdofaznye reaktsii* (Solid-Phase Reactions), Moscow: Khimiya, 1978, p. 360.
12. Nakayama, S., *J. Mater. Sci*., 2001, vol. 6, p. 5643. DOI: 10.1023/A:1012526018348.
13. Morozov, M.I., Lomanova, N.A., and Gusarov, V.V., *Russ. J. Gen. Chem*., 2003, vol. 73, no. 11, p. 1676. DOI: 10.1023/B:RUGC.0000018640.30953.70.
14. Sanchez, C., Rozes, L., Ribot, F., Laberty-Robert, C., Grosso, D., Sassoye, C., Boissiere, C., and Nicole L., *Compt. Rend. Chim*., 2010, vol. 13, nos. 1–2, p. 3. DOI: 10.1016/j.crci.2009.06.001.
15. Gusarov, V.V., *Russ. J. Gen. Chem*., 1997, vol. 67, no. 12, p. 1846.
16. Sytschev, A.E. and Merzhanov, A.G., *Russ. Chem. Rev*., 2004, vol. 73, no. 2, p. 147. DOI: 10.1070/RC2004v073n02ABEH000837.
17. Popkov, V.I. and Almjasheva, O.V., *Russ. J. Appl. Chem*., 2014, vol. 87, no. 2, p. 167. DOI: 10.1134/S1070427214020074.
18. Lomanova, N.A. and Gusarov, V.V., *Nanosystems: Physics, Chemistry, Mathematics*, 2013, vol. 4, no. 5, p. 696.
19. Tugova, E.A. and Karpov, O.N., *Nanosystems: Physics, Chemistry, Mathematics*, 2014, vol. 5, no. 6, p. 854.
20. Gusarov, V.V. and Lomanova, N.A., *Russ. J. Gen. Chem*., 2013, vol. 83, no. 12, p. 2251. DOI: 10.1134/S1070363213120049.
21. Christensen, A.N. and Hazell, R.G., *Acta Chem. Scand*., 1967, vol. 21, p. 481. DOI: 10.3891/acta.chem.scand.21-0481.
22. Balek, V. and Subrt, J., *Pure Appl. Chem*., 1995, vol. 67, no. 11, p. 1839. DOI: 10.1351/pac199567111839.
23. Zhang, P., Navrotsky, A., Guo, B., Kennedy, I., Clark, A.N., Lesher, C., and Liu, Q., *J. Phys. Chem., C*, 2008, vol. 112, no. 4, p. 932. DOI: 10.1021/jp7102337.
24. D'Assuncao, L.M., Giolito, I., and Ionashiro, M., *Thermochim. Acta*, 1989, vol. 137, no. 2, p. 319. DOI: 10.1016/0040-6031(89)87224-7.
25. Hussein, G.A.M., *Thermochim. Acta*, 1994, vol. 244, p. 139. DOI: 10.1016/0040-6031(94)80214-9.
26. Aghazadeh, M., Ghaemi, M., Golikand, A.N., Yousefi, T., and Jangju, E., *Int. Scholar. Res. Network Ceramics*, 2011, vol. 2011, p. 1. DOI: 10.5402/2011/542104.
27. Wang, J., Liu, Q., Xue, D., and Li, F., *J. Mater. Sci. Lett.*, 2002, vol. 21, p. 1059. DOI: 10.1023/A:1016033329184.
28. Saraswat, I., Vajpei, A.C., Garg, V.K., Sharma, V.K., and Prakash, N., *J. Colloid Interface Sci*., 1980, vol. 73, no. 2, p. 373. DOI: 10.1016/0021-9797(80)90083-1.
29. Palchik, O., Felner, I., Kataby, G., and Gedanken, A., *J. Mater. Res*., 2011, vol. 15, no. 10, p. 2176. DOI: 10.1557/JMR.2000. 0313.
30. Gusarov, V.V. and Suvorov, S.A., *Russ. J. Appl. Chem*., 1990, vol. 63, no. 8, p. 1689.
31. Fawcett, T.G., Faber, J., Needham, F., Kabekkodu, S.N., Hubbard, C.R., and Kaduk, J.A., *Powder Diffr*., 2012, vol. 21, no. 2, p. 105. DOI: 10.1154/1.2204958.
32. Young, R.A., *The Rietveld Method*, Oxford: Oxford Univ., 1993, p. 312.
33. Lutterotti, L., Matthies, S., and Wenk, H.R., *Int. Union Crystallogr. Comm. Powder Diffr. Newslett*., 1999, vol. 21, p. 14.